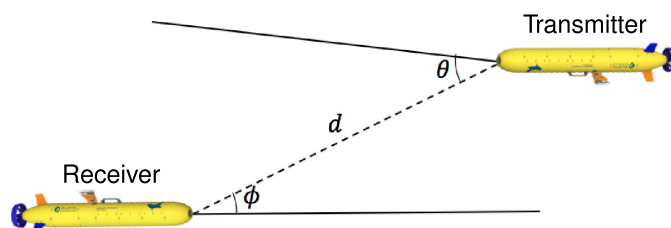# Extended Kalman Filter Based Linear Quadratic Regulator Control for Optical Wireless Communication Alignment

Asem Alalwan, *Graduate Student Member, IEEE*
Tadjine Mohamed
Messaoud Chakir
Taous Meriem Laleg, *Senior Member, IEEE*

Extended Kalman Filter Based Linear Quadratic Regulator Control for Optical Wireless Communication Alignment

Asem Alalwan [1], *Graduate Student Member, IEEE,*
Tadjine Mohamed,[2] **Messaoud Chakir,**[2]
and Taous Meriem Laleg [1], *Senior Member, IEEE*

[1]King Abdullah University of Science and Technology (KAUST), Thuwal 23955-6900, Saudi Arabia
[2]Control Systems and Applied Mathematics, National Polytechnic School ENP of Algiers. 10, St Hacen Badi, El Harrach, Algiers 16200, Algeria

Abstract: High-precision positioning of two underwater mobile robots based on laser beams alignment has been investigated in this work. Usually, the control problem addressed in laser beams aims to maintain the position of the receiver robot aligned with the transmitter robot despite the effects of noise and active disturbances. In this paper, a new state space model is proposed. The latter is more precise than the usual used two state space model [1]. Furthermore, an estimation based control strategy using Extended Kalman Filter Estimator (EKF) and Linear Quadratic Regulator (LQR) is proposed to achieve the control objectives. LQR controller is well known as optimal control design with better tuning flexibility along with intrinsic robustness properties such as noise and output disturbance rejections. The achieved performance of the proposed controller is compared to the conventional proportional (P), Proportional-Integral-Derivative (PID) and Proportional-Integral (PI) controller to analyze the improvements and stability. In addition, an investigation of a sensitivity analysis is conducted to show robustness with different process noise variances of LQR controller.

Index Terms: Control design, extended kalman filter (EKF), linear quadratic regulator (LQR), underwater wireless optical communication (UWOC).

1. Introduction

Over the last decade, many research efforts have been devoted towards advancing Optical Wireless Communication (OWC) technology. OWC is considered to be a potential paradigm in communication area. In fact, compared to Radio Frequency (RF)-based communication systems, OWC is able to provide high security, low cost and high data rates [2]. A form of OWC used for underwater communication is the Visible Light Communication (VLC) where the main advantage of VLC is its ability to provide high-speed, reliable, flexible and cost-effective for underwater wireless communication scheme [3], [4]. In addition, a bidirectional wireless optical communication medium was considered in [5] to transmit ultrahigh definition (UHD) video via a downlink channel and the uplink channel was utilized to receive the feedback messages. Although OWC is more commonly

used than most of the classical communication techniques, an inherent challenge that limits this technology, is to build and keep close-to-line-of-sight links, since the beam signals are highly directional. Specifically, keeping a line-of-sight (LOS) is very challenging due to the fact that when the signal is exposed to the atmosphere or underwater ambient, it is expected to get distorted in its power and hence affects the quality of the transmission [6]. To overcome this, Pointing, Acquisition and Tracking (PAT) has been proposed to maintain LOS for optical wireless communication [7]. In general sense, the PAT system can be seen as a closed-loop control system where sensing devices, controllers and actuators are deployed. An advanced PAT technique was recently proposed in [8] for dynamic optical localization of a mobile robot using Kalman filtering-based position prediction where an light-emitting diode (LED) based system that achieves simultaneous localization and communication (SLAC). Although a large number of research works have been published in the field of wireless communication, a few have been dedicated to device advanced PAT techniques that can overcome air turbulence such as thunderstorms and wind shear [9].

Therefore, several research efforts have been conducted to improve the performance of OWC systems by developing various types of PAT systems. The main objective is to make the PAT system with the following criteria: (a) a quick response, (b) more accuracy, (c) a larger range of tracking, (d) a lower cost, and (f) less complexity. Hence, the development of estimation and control strategies were considered to advance the OWC technology. Specifically, various techniques of control that have been combined with a feedback and/or feedforward closed loop, estimation and/or identification methods like Proportional Integral Derivative (PID) and robust PID controllers. For instance, a PID framework was utilized in [2] to point to a 3D target by only using a 2D sensor for free-space optical communication links. In addition, robust PID algorithms and passive control techniques were devised in [10], [11] to ensure the stability of the transient behavior around the equilibrium points for the case of uniform angular relative motion of a direct-detection cooperative optical beam tracking. In [12], the authors provided a very solid state of art for various types of PID control algorithms for different applications of the PAT system used for wireless communication systems. To overcome the rapid attenuation of optical signals due to spreading loss, scattering, and absorption in free space communication, adaptive PID algorithms were proposed in [13], [14]. Another framework was proposed in [15] for laser communication terminals to keep both the communication partners precisely aligned as well as angle at which the transmitted signal is received.

The aforementioned PID controllers have been proposed to generally maximize the optical signal detected by a photodiode using a voice-coil motor actuator and stabilize a beam at a desired angle. Many researchers have shown that the PID controllers can achieve acceptable performance for stabilizing the optical beam with short settling time. However these conventional control strategies fail to deliver good performance especially under vibration conditions of the pointing systems due to active disturbances. It is difficult to have satisfactory performance covering the total range of disturbance without external compensation using conventional PID controller because of the significant variations in the amplitude vibration affected by the external disturbances. Thereafter, it is desirable to design optimal and robust control strategies that can guarantee the closed-loop stability despite of the presence of external disturbances. In addition, practical constraints such as the amount of energy used to control the OWC systems is a matter of great importance in the communication industry. Therefore, it is important to construct an optimal control paradigm that can optimize an objective function that reflects directly both the energy usage and keeping the line-of-sight in the desired position.

In this paper, we propose an extension on the model given in [1] that describes alignment of two mobile robot in an underwater communication framework. Our model shows more realistic behaviour in which we have two degree of freedom to control the angular velocity that will lead to stabilize the position of the two transceivers. We designed Extended Kalman Filter (EKF) for estimating the voltage received, position, and angular velocity since we do not have access to all states. Then we applied Linear Quadratic Regulator (LQR) controller to stabilize the system at a desired point.

To validate the performance of our control design the simulation results was compared to the proportional (P) controller, proportional integral (PI) controller, and PID controller.
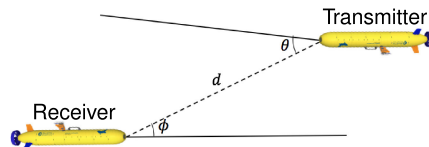
Fig. 1. Relative orientation between the transmitter and receiver.

This paper is organized as follows. In Section 2, the optical transceiver dynamical system is explained and the control problem is introduced. In Section 3, the design of EKF based LQR algorithms are given. Numerical simulation results are illustrated and discussed in Section 4 followed by stability analysis in Section 4.1. Finally, concluding remarks were shown in Section 5.

2. System Description And Dynamical Models

Optical communication consist of transmitter and receiver. It starts at the transmitter by converting the electrical signal to an optical signal. This signal passes through the channel and is received at the receiver end by converting the light signal to an electrical signal again. Underwater Wireless Optical Communication (UWOC) channels have several unique characteristics compared with terrestrial FSO communication channels. The existing terrestrial models of FSO channel are not adequate for underwater ambiance; thus, a new study for reliable models of the channels must be considered. We firstly have to understand basic properties of light propagation in underwater in order to to derive new channel models for underwater environment.

The water's optical properties are categorized into Inherent Optical Properties (IOPs) and Apparent Optical Properties (AOPs). The former depends on the medium itself and particulate substances with it [16] while the latter depends additionally to the geometrical structure of the light such as diffusion and collimation [16]. On one hand, the main IOPs of water are absorption coefficient, the scattering coefficient,the attenuation coefficient, and the volume scattering function [17]. On the other hand, the major AOPs of water are radiance, irradiance and reflectance [17]. In UWOC system, IOPs are usually used to get the communication link budgets, while AOPs are used in determining ambient light levels for communication systems near the ocean surface [16]. To this end, we will focus on IOPs thought the concepts of absorption and scattering coefficients as well as Beer Lamberts law. These notions deliver a theoretical basis for UWOC channel models [18]. The optical signal in an UWOC link initialized from the transmitter will experience different losses before reaching the receiver. They encompass system loss that comes from the transceivers, link losses by water attenuation, water turbulence and geometric misalignment. In this framework, we will introduce the light intensity model for the channel as well as the state-space model representation for estimation and control problem.

The light intensity model of the optical system has been adjusted from [19]. This model includes all components transmitter and receiver circuitries, amplifiers, lenses, photodiodes and LED. Figure 1 shows the orientation between the transmitter and receiver in which we focus on the transmission angle, the angle of incidence and the transmission distance d as variables of interest.

The angular intensity distribution of the transmitter is symmetric about the normal ($\theta = 0°$). Hence, intensity of the transmitter at different angles can be computed if the light intensity of the normal is known based on the spatial intensity curve l_θ. Maximum intensity received on the normal direction $\theta = 0°$ and it decreases as θ increases in both directions. We note that l_θ can be taken from the LED vendor or experimentally measured data.

To describe the spreading of the optical channel, it is to be considered as spherical model with exponential decay [20], and let c be the attenuation coefficient for the channel in which the light is sent. Beers law gives signal degradation at distance d caused by absorption $\tilde{A}$
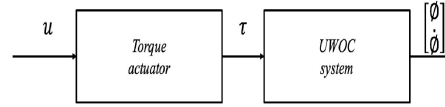
$$\tilde{A} = \exp(-cd). \tag{1}$$

Fig. 2. Actuator block diagram.

The equation of the irradiance reaching the receiver can be shown by combining the spherical spreading with the exponential decay.

$$E_\theta(d) = I_\theta \exp(-cd)/d^2. \tag{2}$$

Finally, the power of the signal irradiance at receiver can be computed by the following equation

$$P_{in} = E_\theta(d)A_0 \cos(\phi), \tag{3}$$

where ϕ is the angle considered from the receiver normal to the the transmitter and A_0 is the area of the receiver. The photodiode emits current once the light hits the receiver, which then gets filtered and amplified, to be processed by an analog-digital converter. After all the steps, the full signal received model can be shown as [1]

$$V_d = C_p I_\theta \exp(-cd)\cos(\phi)/d^2, \tag{4}$$

where V_d is the voltage received and C_p is a constant constant depending on different parameters related to the filter, amplifier circuits, and area of the detector.

2.1 State-Space Formulation and Analysis

We have extended the model [1] from two state to three state model. The new augmented LED-based optical communication model that we propose uses the velocity as an additional state variable to develop a force-velocity based controller to ensure the stability of the closed-loop system. This model offers a direct relationship between the position and the velocity. Furthermore, the proposed force-velocity based controller can easily be actuated because it has the same properties as the position-based controller. Moreover it has two degrees of freedom that can help in better tuning for the control action (see Figure 2).

The state space representation is formulated based on the four variables of interest d, θ, ϕ, and $\dot{\phi}$ that relates to the voltage received, the angles of the transmitter and receiver and the velocity of the receiver actuator. However, we note that practically it is not easy to move the distance d in a desirable way because it needs to move the whole robot. Effectively, controlling the position ϕ is more practical since it is more independent and is based on a local decision. The aim is to adjust the ϕ angle to zero in order to get alignment for both transceivers robots in each side of communication. We combine θ and d in one state variable x_1 as we discussed before that d can not be adjusted easily. Thus, our state variables are defined as follows

$$\mathbf{x} = \begin{bmatrix} x_1 \\ x_2 \\ x_3 \end{bmatrix} = \begin{bmatrix} C_p I_\theta e^{-cd}/d^2 \\ \phi \\ \dot{\phi} \end{bmatrix}. \tag{5}$$

As in (5) we assume that the dynamic is slow which can be taken with a Gaussian process. The representation in discrete time domain is shown below

$$\mathbf{x_k} = \begin{bmatrix} x_{1,k} \\ x_{2,k} \\ x_{3,k} \end{bmatrix} = \begin{bmatrix} x_{1,k-1} + w_{1,k-1} \\ x_{2,k-1} + x_{3,k-1} + w_{2,k-1} \\ x_{3,k-1} + u_{k-1} + w_{3,k-1} \end{bmatrix}, \tag{6}$$

where $w_{1,k}$, $w_{2,k}$ and $w_{3,k}$ are the process noise which is assumed to be Gaussian, independent and white noises. The u_k is the control input in which the receiver velocity is adapted in order to

control the position ϕ. The measurement $V_{d,k}$ is expressed as

$$V_{d,k} = x_{1,k}g(x_{2,k}) + v_k, \tag{7}$$

where g is cosine function and v_k is an additive white Gaussian noise. The aim of the estimation is to get x_2 and x_3 that will guide the controller to the normal direction $\phi = 0°$.

3. Estimation and Control Design

The Kalman filter is an optimal filter with regards to minimizing square error based on the sensor readings and their variances of the variance readings. The theory behind a Kalman filter requires that the system equations included in the Kalman filter algorithm are linear. Different types of versions of the original Kalman filter have been used to implement the Kalman filter on problems that are close to linear while still achieving close to optimal performance due to the fact that the Kalman filter only works for linear systems. Most of real world applications are nonlinear including mobile, ground and underwater robots. Linearized Kalman Filter (LKF), Extended Kalman Filter (EKF) or Unscented Kalman Filter (UKF) are commonly used for nonlinear estimation. EKF is most popular in many applications where it achieves better performance [21] with less computation cost compared with UKF. Thus, we first design EKF that can deal with the nonlinearities at the output. The estimation and alignment algorithm are explained as follows.

From (6), the matrices A and B are given as follows:

$$A = \begin{bmatrix} 1 & 0 & 0 \\ 0 & 1 & 1 \\ 0 & 0 & 1 \end{bmatrix}, \qquad B = \begin{bmatrix} 0 \\ 0 \\ 1 \end{bmatrix} \tag{8}$$

with a linearized output, the observability matrix $\mathcal{O}$ is

$$\mathcal{O} = \begin{bmatrix} C \\ CA \\ CA^2 \end{bmatrix} \tag{9}$$

In (9), we performed the linearization for the output function by taking the derivative of the nonlinear output function with respect to space and evaluated at the steady-state which is zero. The matrix C is defined in (7) which in fact implies that the observability matrix will not be full rank. As a result, two different measurement of light intensity is necessary to achieve local observability. The possible solutions are, to use two receivers with different orientation or to incorporate a scanning technique with a motor rotating slowly around a mean position. The latter solution avoid complexity and cost so the control input drive x_2 to zero position. The measurement is taken in a step of $2°$ and at least two measurements are needed to form the y vector.

$$y_k = \begin{bmatrix} x_{1,k}\cos(x_{2,k}) + v_k \\ x_{1,k-1}\cos(x_{2,k-1}) + v_{k-1} \end{bmatrix} \tag{10}$$

The EKF algorithm is explained as follows. We first define an array of angles which contain a predefined angles $\psi_k = \{-2, -4, -6, -8, -10, -8, -6, -4, -2, 0, 2, 4, 6, 8, 10, 8, 6, 4, 2, 0\}$. In each iteration one angle ψ_k is chosen sequentially. P, Q_{EKF} and R_{EKF} are three covariance matrices related to the EKF. P is the conditional error covariance matrix in which it should be initialized with a positive definite matrix. Q_{EKF} and R_{EKF} should also be positive definite and diagonal matrices. The former correspond to the process noise covariance, and the latter to the measurement covariance matrix.

3.1 Extended Kalman Filter Algorithm

- Prediction:

$$\begin{cases} \hat{x}_{1,k} = \hat{x}_{1,k-1} \\ \hat{x}_{2,k} = \hat{x}_{2,k-1} + \hat{x}_{3,k-1} \\ \hat{x}_{3,k} = \hat{x}_{3,k-1} + u_{k-1} \end{cases} \tag{11}$$

$$P_k = AP_{k-1}A^T + Q_{\text{EKF}} \tag{12}$$

- Output measurements and estimated output measurements:

$$y_k = \begin{bmatrix} V_{d,k} \\ V_{d,k-1} \end{bmatrix} \tag{13}$$

$$\hat{y}_k = \begin{bmatrix} \hat{x}_{1,k} \cos(\hat{x}_{2,k} + \psi_k) \\ \hat{x}_{1,k-1} \cos(\hat{x}_{2,k-1} + \psi_{k-1})) \end{bmatrix} \tag{14}$$

with (11) $\hat{y}$ can be rewritten as:

$$\hat{y}_k = h(\hat{x}_{1,k}, \hat{x}_{2,k}, u_{k-1})$$

$$= \begin{bmatrix} \hat{x}_{1,k} \cos(\hat{x}_{2,k} + \psi_k) \\ \hat{x}_{1,k} \cos(\hat{x}_{2,k} - \hat{x}_{3,k} + u_{k-1} + \psi_{k-1})) \end{bmatrix} \tag{15}$$

C matrix can be computed from the Jacobian matrix as:

$$C_k = \frac{\partial h(\hat{x}_{1,k}, \hat{x}_{2,k}, \hat{x}_{3,k}, u_{k-1})}{\partial x_k}$$

$$= \begin{bmatrix} C_{k,1,1} & C_{k,1,2} & 0 \\ C_{k,2,1} & C_{k,2,2} & C_{k,2,3} \end{bmatrix} \tag{16}$$

where,

$$\begin{aligned} C_{k,1,1} &= \cos(\hat{x}_{2,k} + \psi_k) \\ C_{k,1,2} &= -\hat{x}_{1,k} \sin(\hat{x}_{2,k} + \psi_k) \\ C_{k,2,1} &= \cos(\hat{x}_{2,k} - \hat{x}_{3,k} + u_{k-1} + \psi_{k-1}) \\ C_{k,2,2} &= -\hat{x}_{1,k} \sin(\hat{x}_{2,k} - \hat{x}_{3,k} + u_{k-1} + \psi_{k-1}) \\ C_{k,2,3} &= \hat{x}_{1,k} \sin(\hat{x}_{2,k} - \hat{x}_{3,k} + u_{k-1} + \psi_{k-1}) \end{aligned} \tag{17}$$

- Update:

$$K_k = P_k C^T (CP_k C^T + R_{\text{EKF}})^{-1} \tag{18}$$

$$\hat{x}_k = \hat{x}_k + K_k(y_k - \hat{y}_k) \tag{19}$$

$$P_k = (I - K_k C_k)P_k \tag{20}$$

- The control is computed as

$$u_k = -G_1 \hat{x}_{2,k} - G_2 \hat{x}_{3,k} \tag{21}$$

where G_1 and G_2 are positive gains.

Two important conditions for convergence of the EKF. First, the non-singularity of the observability matrix and initial conditions of the state estimates should be sufficiently small for EKF to work.
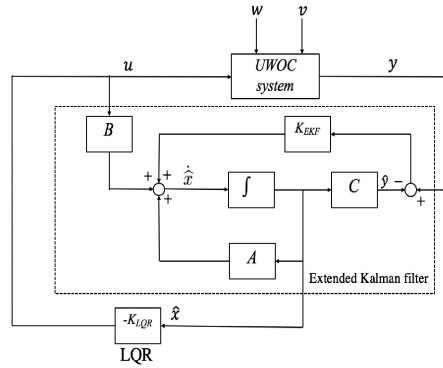
Fig. 3. Proposed control system.

3.2 LQR Control Design

The system dynamics (6), and the disturbance signals are stochastic with known Gaussian statistical properties.

The LQR control problem is based on searching for the optimal control which minimizes the pointing error. This pointing problem can be interpreted as finding a set-point $u = -K_{LQR}x$ that minimizes the following discrete cost function

$$J_{LQR} = \frac{1}{2} \sum_{k=0}^{\infty} \left(x_k^T Q_{LQR} x_k + u_k^T R_{LQR} u_k \right). \tag{22}$$

where Q_{LQR} and R_{LQR} are positive definite symmetric weighting matrices. The cost function compromises between minimizing tracking error and minimum energy effort in which Q_{LQR} and R_{LQR} can be adjusted. The states of the system are considered to be not measurable and will be estimated using EKF. From computational point of view, the LQR design depends on solving two Riccati equations corresponding to the EKF design and on the LQ controller design. EKF based on LQR controller requires two steps: firstly, to search for optimal control to the linear quadratic regulator (LQR) problem. Then to find an optimal estimate for EKF design. The required solution to the LQR problem is then found by replacing the actual state to its estimate. Hence, from the separation principle the LQR problem and its solution can be separated into two different parts, as shown in Figure 3.

Optimal state feedback. Given the system: $x_{k+1} = Ax_k + Bu_k$ with a non-zero initial states $x(0)$, find the input signal u_k which takes the x_2 and x_3 to the zero state in an optimal way, *i.e.* by minimizing the discrete cost function (22). The optimal solution (for any initial state) is $u_k = -K_{LQR}x_k$, where

$$K_{LQR} = (B^T X B + R_{LQR})^{-1}(B^T X A), \tag{23}$$

where $X = X^T \geqslant 0$ is the unique positive-semidefinite solution of the algebraic Riccati equation

$$A^T X A - X - (A^T X B)(B^T X B R_{LQR})^{-1}(B^T X A) + Q_{LQR} = 0. \tag{24}$$

The EKF states is computed as explained in Section 3.1 and with the optimal K_{LQR} the computed control of LQR is

$$u_k = -K_{LQR} \begin{bmatrix} \hat{x}_{2,k} \\ \hat{x}_{3,k} \end{bmatrix}. \tag{25}$$

4. Numerical Simulations

In this section we will examine the design of EKF based LQR control algorithm according to the simulation parameters given in Table 1. We firstly compare the Proportional (P) controller algorithm

TABLE 1
System Parameters

Parameters	value
Q_{sys}	$\begin{bmatrix} 0.0025 & 0 & 0 \\ 0 & .0025 & 0 \\ 0 & 0 & 0.0025 \end{bmatrix}$
R_{sys}	0.001
P_0	$\begin{bmatrix} 100 & 0 & 0 \\ 0 & 100 & 0 \\ 0 & 0 & 100 \end{bmatrix}$
Q_{EKF}	$\begin{bmatrix} 0.0025 & 0 & 0 \\ 0 & 0.0025 & 0 \\ 0 & 0 & 0.0025 \end{bmatrix}$
R_{EKF}	$\begin{bmatrix} 1 & 0 \\ 0 & 1 \end{bmatrix}$
Q_{LQR}	$\begin{bmatrix} 30 & 0 \\ 0 & 1 \end{bmatrix}$
R_{LQR}	1000
$\hat{x}_0$	$[5, 2, 3]^T$
G (proportional gain)	$[.1, 0.4]$
K_{LQR}	$[0.1287, 0.5764]$

TABLE 2
RMSE Between Controlled States and Desired Reference

Estimation based control algorithm	$\hat{x}_2$	$\hat{x}_3$
LQR controller	0.7886	0.2416
P controller	0.9313	0.2628
Improvement	18.09%	8.77%

to the LQR controller. Figure 4 shows the states of the underwater transceiver system, from which it can be seen the convergence of both x_2 and x_3 are asymptotically going to zero in two seconds by LQR while it takes almost three seconds in P controller. In addition, it can be seen in Figure 4 the convergence between estimate and actual state x_1 that describes the voltage received at the receiver end. In Table 2 the the Root Mean Square Error RMSE of the both controllers related the stabilization point in which there is around 8.77% improvement using LQR controller in the velocity state x_3 while there is an improvement of 18.09% in terms of position x_2. Next, a sensitivity analysis is considered as well where different values for the variance of the process noise w are employed to the closed-loop system to investigate the numerical stability of the proposed framework. Figure 5 applies the following three values of process noise variances $\sigma_1 = 0.00025$, $\sigma_1 = 0.0005$ and $\sigma_1 = 0.001$. As it can be seen the actual and estimated position state (i.e., x_2 and $\hat{x}_2$) are able to reach zero under the proposed EKF-LQR algorithm as process noise variances increases.
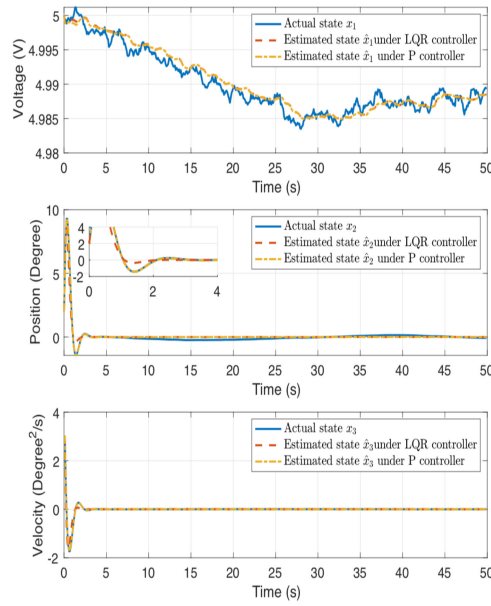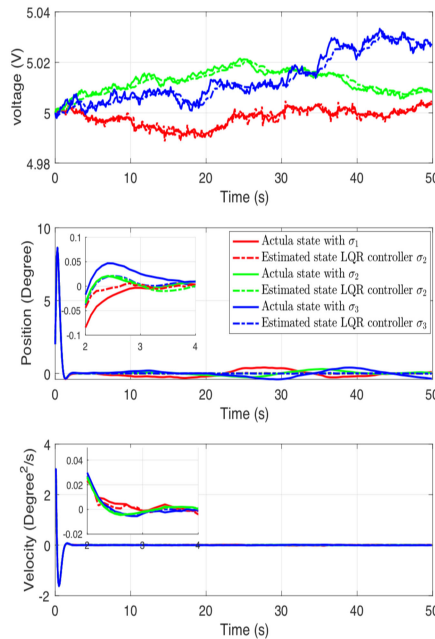
Fig. 4. Closed-loop state profile x_1, x_2, and x_3.

Fig. 5. Closed-loop state profile x_1, x_2, x_3 with different process noises $\sigma_{1,2,3}$.

Finally, we show the performance of PI,PID, and LQR controller and our observations in different PID gains. In figure 6 and 7 we see clearly closed-loop state profile x_2 and x_3 with PI controller and PID in which the settling time was faster when adding the derivative gain K_d. Also, by varying the K_i in figure 8 and 7 we could overcome the overshoot in both x_2 and x_3. Generally, the LQR controller was outperforming in comparison with P,PI, and PID.
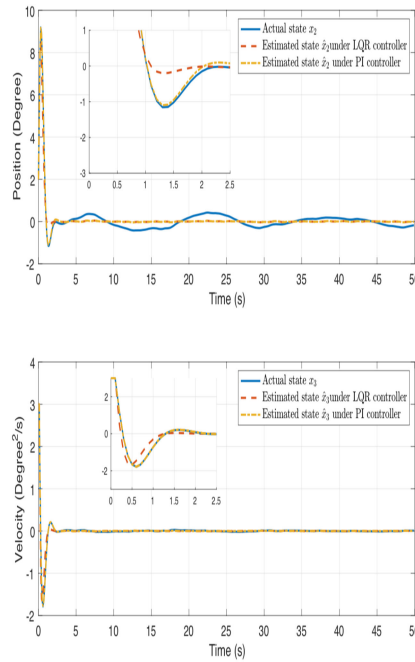
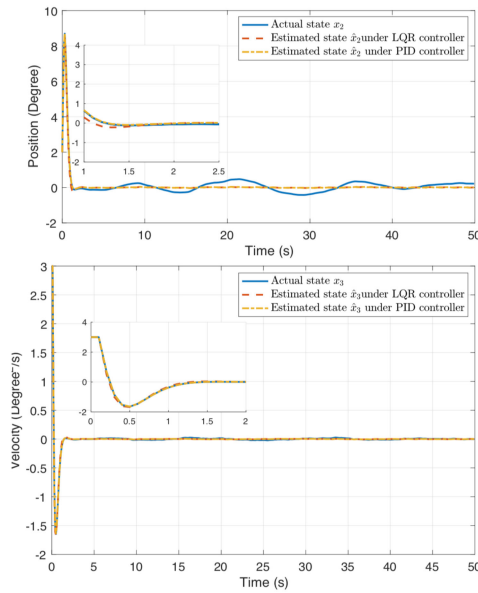Fig. 6. Closed-loop state profile x_2 and x_3 with PI controller.

Fig. 7. Closed-loop state profile x_2 and x_3 with PID controller.

4.1 Stability and Trajectories Analysis

The new augmented LED-based optical communication model (5) that we propose in Section 2 uses the velocity as additional state variable and a force-velocity control to ensure the closed-loop stability of the system. Since the state velocity and force/torque velocity control have not yet been considered in [1], this proposed model (5) presents direct relationship between the position
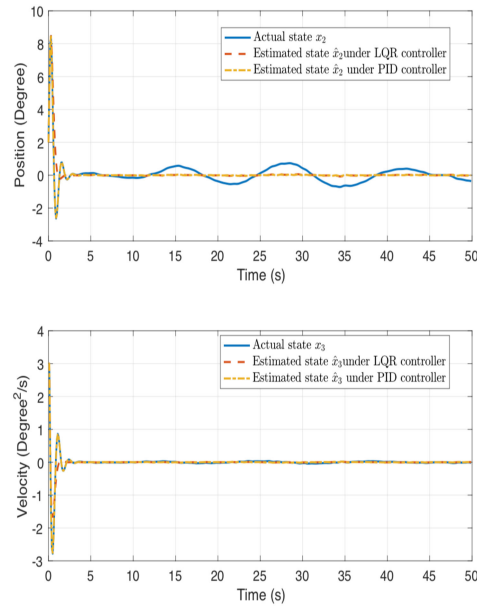
Fig. 8. Closed-loop state profile x_2 and x_3 with PID controller with overshoot.
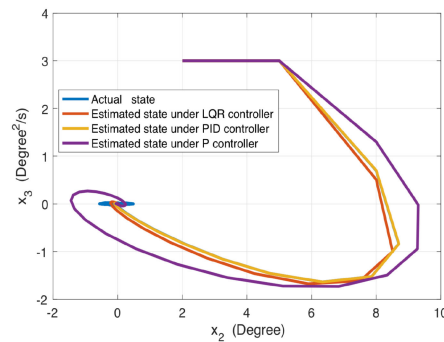

Fig. 9. Phase portrait analysis: velocity vs positions under LQR, PID, and P controllers.

and velocity states. Furthermore, the proposed force-velocity control has similarities with the force position input and helps to design a flexible mechanical structure with a velocity actuator device.

The phase portrait provides the analysis of the stability trajectories to the equilibrium points [22]. Figure 9 shows the phase portrait analysis of the velocity versus position under the LQR, PID, and P controller. It can be seen that the trajectories of both actual and estimated states drive to a stable focus around the equilibrium point zero while it takes more time to converge for P controller comparing to both LQR and PID controller.

5. Conclusion

In this paper, a new model has been proposed to control the alignment of a two underwater mobile robot optical transceiver such that the angle from the receiver normal to the line connecting the receiver with the transmitter is stabilized to zero even in the presence of active disturbance and noise based on LQR controller with EKF. The performance of the presented LQR based EKF controller has been evaluated in a closed loop and it has been compared to the conventional P controller, PI controller and PID controller. The simulation results demonstrated that the LQR based

EKF controller is more effective relatively than the rest of controllers, while it preserves its simplicity in tuning parameters. However, the inclusion of the integral controller (i.e., PI and PID) was able to reduce the overshoot of the closed-loop state. Furthermore, a sensitivity analysis was conducted where different values of the process noise variance were employed to investigate the numerical robustness of the proposed work. In addition, the stability trajectories have been analysed using the phase plane analysis of LQR,PID and P controller. Finally, as a future work we would like to validate our algorithms experimentally and further describe other effects or disturbances in real Under Water Optical Communication (UWOC) scenarios such as bubbles of the water, signal blockage, water turbidity, etc.

References

[1] P. B. Solanki, M. Al-Rubaiai, and X. Tan, "Extended kalman filter-based active alignment control for led optical communication," *IEEE/ASME Trans. Mechatronics*, vol. 23, no. 4, pp. 1501–1511, Aug. 2018.

[2] T.-H. Ho, "Pointing acquisition and tracking systems for free-space optical communication links," Ph.D. dissertation, Dept. Elect. Comput. Eng., University of Maryland, College Park, MD, USA, 2007.

[3] S. Hessien, S. C. Tokgöz, N. Anous, A. Boyacı, M. Abdallah, and K. A. Qaraqe, "Experimental evaluation of OFDM-based underwater visible light communication system," *IEEE Photon. J.*, vol. 10, no. 5, Oct. 2018, Art. no. 7907713.

[4] P. B. Solanki, S. D. Bopardikar, and X. Tan, "A bidirectional alignment control approach for planar led-based free-space optical communication systems," in *Proc. IEEE/ASME Int. Conf. Adv. Intell. Mechatronics (AIM)*, 2020, pp. 1949–1955.

[5] A. Al-Halafi and B. Shihada, "UHD video transmission over bidirectional underwater wireless optical communication," *IEEE Photon. J.*, vol. 10, no. 2, 2018, Art. no. 7902914.

[6] A. G. Nasser and M. A. A. Ali, "Performance of LED for line-of-sight (LoS) underwater wireless optical communication system," *J. Opt. Commun.*, to be published, doi: 10.1515/joc-2020-0132.

[7] P. Deng, T. Kane, and O. Alharbi, "Reconfigurable free space optical data center network using gimbal-less MEMS retroreflective acquisition and tracking," in *Proc. Free-Space Laser Commun. Atmospheric Propag. XXX*, vol. 10524, 2018, Art. no. 1052403.

[8] J. N. Greenberg and X. Tan, "Dynamic optical localization of a mobile robot using Kalman filtering-based position prediction," *IEEE/ASME Trans. Mechatronics*, vol. 25, no. 5, pp. 2483–2492, Oct. 2020.

[9] M. Elamassie and M. Uysal, "Performance characterization of vertical underwater vlc links in the presence of turbulence," in *Proc. 11th Int. Symp. Commun. Syst., Netw. Digital Signal Process.*, 2018, pp. 1–6.

[10] G. Marola, D. Santerini, and G. Prati, "Stability analysis of direct-detection cooperative optical beam tracking," *IEEE Trans. Aerosp. Electron. Syst.*, vol. 25, no. 3, pp. 325–334, May 1989.

[11] A. K. Majumdar and J. C. Ricklin, *Free-Space Laser Communications: Principles and Advances*, vol. 2. Berlin, Germany: Springer, 2010.

[12] Y. Kaymak, R. Rojas-Cessa, J. Feng, N. Ansari, and M. Zhou, "A survey on acquisition, tracking, and pointing mechanisms for mobile free-space optical communications," *IEEE Commun. Surveys Tut.*, vol. 20, no. 2, pp. 1104–1123, Apr.–Jun. 2008.

[13] C. Pontbriand, N. Farr, J. Ware, J. Preisig, and H. Popenoe, "Diffuse high-bandwidth optical communications," in *Proc. OCEANS*, 2008, pp. 1–4.

[14] C. Lu, C. Li, and Z. Xu, "Experimental investigation of underwater weak optical communication using a photomultiplier tube receiver," in *Proc. Asia Commun. Photon. Conf.*, 2018, pp. 1–3.

[15] C. Schmidt and J. Horwath, "Wide-field-of-regard pointing acquisition and tracking-system for small laser communication terminals," in *Proc. Int. Conf. Space Opt. Syst. Appl.*, 2012, pp. 1–6.

[16] L. J. Johnson, F. Jasman, R. J. Green, and M. S. Leeson, "Recent advances in underwater optical wireless communications," *Underwater Technol.*, vol. 32, no. 3, pp. 167–175, 2014.

[17] R. W. Spinrad, K. L. Carder, and M. J. Perry, *Ocean Optics*. London, U.K.: Oxford Univ. Press, 1994, vol. 25.

[18] C. Gabriel, M. A. Khalighi, S. Bourennane, P. Leon, and V. Rigaud, "Channel modeling for underwater optical communication," in *Proc. Globecom Workshops*, 2011, pp. 833–837.

[19] M. Doniec, M. Angermann, and D. Rus, "An end-to-end signal strength model for underwater optical communications," *IEEE J. Ocean. Eng.*, vol. 38, no. 4, pp. 743–757, Oct. 2013.

[20] F. Miller, A. Vandrome, and J. McBrewster, *Beer-Lambert Law*. Saarbrücken, Germany: VDM Publishing, 2009.

[21] J. Simanek, "Data fusion for localization using state estimation and machine learning," Ph.D. dissertation, Dept. Elect. Eng. Inform. Technol., University Czech Technical, Prague, Czechia, 2015.

[22] J.-J. E. Slotine *et al.*, *Applied Nonlinear Control*, vol. 199, Englewood Cliffs, NJ, USA: Prentice Hall, 1991.